Plant Physiology and Biochemistry 210 (2024) 108612

Contents lists available at ScienceDirect

Plant Physiology and Biochemistry

journal homepage: www.elsevier.com/locate/plaphy

# Characterization of cinnamate 4-hydroxylase (CYP73A) and *p*-coumaroyl 3′-hydroxylase (CYP98A) from *Leucojum aestivum*, a source of Amaryllidaceae alkaloids

Vahid Karimzadegan [a], Manoj Koirala [a], Sajjad Sobhanverdi [a], Natacha Merindol [a], Bharat Bhusan Majhi [a], Sarah-Eve Gélinas [a], Vitaliy I. Timokhin [b], John Ralph [b,c], Mehran Dastmalchi [d], Isabel Desgagné-Penix [a,*]

[a] Department of Chemistry, Biochemistry and Physics, Université Du Québec à Trois-Rivières, Trois-Rivières, Québec, Canada
[b] Department of Energy's Great Lakes Bioenergy Research Center, Wisconsin Energy Institute, Madison, WI, 53726, USA
[c] Department of Biochemistry, University of Wisconsin-Madison, Madison, WI, 53706, USA
[d] Department of Plant Science, McGill University, Montréal, Québec, Canada

ARTICLE INFO

*Keywords:*
Phenylpropanoids
Specialized metabolism
Ascorbate peroxidase/4-coumarate 3-hydroxylase
Endoplasmic reticulum membrane localization
Coumaric acid
Metabolic profile

ABSTRACT

Biosynthesis of Amaryllidaceae alkaloids (AA) starts with the condensation of tyramine with 3,4-dihydroxybenzaldehyde. The latter derives from the phenylpropanoid pathway that involves modifications of *trans*-cinnamic acid, *p*-coumaric acid, caffeic acid, and possibly 4-hydroxybenzaldehyde, all potentially catalyzed by hydroxylase enzymes. Leveraging bioinformatics, molecular biology techniques, and cell biology tools, this research identifies and characterizes key enzymes from the phenylpropanoid pathway in *Leucojum aestivum*. Notably, we focused our work on *trans*-cinnamate 4-hydroxylase (*Lae*C4H) and *p*-coumaroyl shikimate/quinate 3'-hydroxylase (*Lae*C3′H), two key cytochrome P450 enzymes, and on the ascorbate peroxidase/4-coumarate 3-hydroxylase (*Lae*APX/C3H). Although *Lae*APX/C3H consumed *p*-coumaric acid, it did not result in the production of caffeic acid. Yeasts expressing *Lae*C4H converted *trans*-cinnamate to *p*-coumaric acid, whereas *Lae*C3′H catalyzed specifically the 3-hydroxylation of *p*-coumaroyl shikimate, rather than of free *p*-coumaric acid or 4-hydroxybenzaldehyde. *In vivo* assays conducted *in planta* in this study provided further evidence for the contribution of these enzymes to the phenylpropanoid pathway. Both enzymes demonstrated typical endoplasmic reticulum membrane localization in *Nicotiana benthamiana* adding spatial context to their functions. Tissue-specific gene expression analysis revealed roots as hotspots for phenylpropanoid-related transcripts and bulbs as hubs for AA biosynthetic genes, aligning with the highest AAs concentration. This investigation adds valuable insights into the phenylpropanoid pathway within Amaryllidaceae, laying the foundation for the development of sustainable production platforms for AAs and other bioactive compounds with diverse applications.

## 1. Introduction

The Amaryllidaceae are pharmacologically potent plant species owing to the production of phyla-restricted specialized metabolites, namely the Amaryllidaceae alkaloids (AAs) (Hotchandani and Desgagne-Penix, 2017; Tallini et al., 2017; Jayawardena et al., 2024; Ka et al., 2020). The structurally diverse alkaloids derived from this family are associated with a multitude of pharmacological applications. *Leucojum aestivum* L. (Summer snowflake) of the Amaryllidaceae family is a reported source of galanthamine, an AA approved as a treatment for mild symptoms of Alzheimer's disease (Berkov et al., 2009). The plant additionally accumulates anticancer and antiviral lycorine- and haemanthamine-type AAs (Liu et al., 2004; Havelek et al., 2014; Girard et al., 2022). However, due to their variable and low abundance in nature, extraction from plants would pose a threat to their habitats and to the growth of native plants (Berkov et al., 2009). Microbial platforms, such as bacteria or yeast, offer promising alternatives for producing valuable plant-derived compounds through synthetic biology

* Corresponding author. Department of Chemistry, Biochemistry and Physics, Université du Québec à Trois-Rivières, 3351 boul. des Forges, Trois-Rivières, QC, G9A 5H7, Canada.
*E-mail address:* Isabel.Desgagne-Penix@uqtr.ca (I. Desgagné-Penix).

https://doi.org/10.1016/j.plaphy.2024.108612
Received 27 November 2023; Received in revised form 29 March 2024; Accepted 4 April 2024
Available online 6 April 2024

approaches (Koirala et al., 2022; Diamond and Desgagne-Penix, 2016). For example, vinblastine, an important anti-cancer drug, was successfully reconstituted in *Saccharomyces cerevisiae* (Zhang et al., 2022). Such an approach requires complete resolution of pathways prior to reassembly in heterologous hosts.

The biosynthesis of AAs starts with the condensation of 3,4-dihydroxybenzaldehyde (DHBA), resulting from the phenylpropanoid pathway, and tyramine that is formed through the decarboxylation of tyrosine (Desgagné-Penix, 2021). The phenylpropanoid core pathway starts with the synthesis of *trans*-cinnamic acid from phenylalanine by the well-characterized cytosolic enzyme phenylalanine ammonia-lyase (PAL) (Fig. 1). The hydroxylation of *trans*-cinnamic acid to *p*-coumaric acid in the early phenylpropanoid pathway is a key step, catalyzed by a cytochrome P450 (CYP450) enzyme, *trans*-cinnamate 4-hydroxylase (C4H), that belongs to the CYP73A subfamily (Khatri et al., 2023). Considering the pivotal role of *p*-coumaric acid derivatives in plant metabolism, structure, development, and defense (Zhang et al., 2020), the catalytic role of C4H is of a great importance. The hydroxylation of *trans*-cinnamic acid into *p*-coumaric acid is expected to be catalyzed by a C4H enzyme in *L. aestivum* as evidenced by similar enzymatic characterizations in various plant species such as liverworts (Liu et al., 2017), Madagascar periwinkles (Hotze et al., 1995), poplars (Ro et al., 2001), and other plants (Chen et al., 2011; Schilmiller et al., 2009). To date, two studies have isolated and partially characterized C4H from Amaryllidaceae species, reporting that the overexpression in bacteria of truncated C4H from *Lycoris radiata* and *L. aurea* yielded *p*-coumaric acid (Li et al., 2018a, 2018b).

From *p*-coumaric acid to caffeic acid, two routes have been suggested (Fig. 1). It was first proposed that direct hydroxylation at the acid level could be catalyzed by a CYP98A family enzyme, as described following heterologous expression of *Arabidopsis thaliana At*CYP98A (referred to as C3H in the presence of *p*-coumaric acid) in the cyanobacterium *Synechocystis* spp. (Xue et al., 2014). A later report suggested that hydroxylation by *At*CYP98A rather occurred via *p*-coumarate esters, including *p*-coumaroyl shikimate and *p*-coumaroyl quinate (referred to as C3′H in the presence of coumarate esters) (Schoch et al., 2001). Recent research indicates that substrate specificity of angiosperm C3′H varies between species and between isoforms of the same species, some displaying promiscuity and favoring *p*-coumaroyl shikimate and *p*-coumaroyl quinate as substrates over various natural and non-natural compounds, including prenyl-, isoprenyl-, benzyl-, and threonyl-coumarates (Alber et al., 2019). On the other hand a bifunctional ascorbate peroxidase/4-coumarate 3-hydroxylase (APX/C3H), a soluble enzyme purified from multiple plant species including *A. thaliana*, maize, and *Brachypodium*, was reported to catalyze the direct hydroxylation of free *p*-coumaric acid to caffeic acid (Barros et al., 2019). A recent study challenged this hypothesis when testing the activity of APX/C3H from *Sorghum bicolor* on *p*-coumaric acid (Zhang et al., 2023a). Caffeic acid can potentially yield DHBA to be incorporated into Amaryllidaceae alkaloids, but the enzyme catalyzing the reaction has not yet been identified.

Here, we report the isolation and functional characterization of C4H, APX/C3H, and C3′H from the AA-producing *L. aestivum* (*Lae*). Heterologous expression of soluble *Lae*APX/C3H was conducted in *Escherichia coli.* Recombinant *Lae*C4H and *Lae*C3′H were expressed in a yeast expression system. The subcellular localization of *Lae*C4H and *Lae*C3′H fusion proteins, and their enzymatic activities were investigated in *Agrobacterium*-infiltrated *Nicotiana benthamiana* plants. *L. aestivum* tissue-specific expression patterns of *LaeC4H* and *LaeC3′H*, and other transcripts involved in the phenylpropanoid, and AA pathways were investigated, and compared with targeted metabolite profiles. This study reports on C4H (CYP73A), APX/C3H and C3′H (CYP98A) from the Amaryllidaceae family to clarify their role in the phenylpropanoid pathway upstream of the AA biosynthetic pathway.

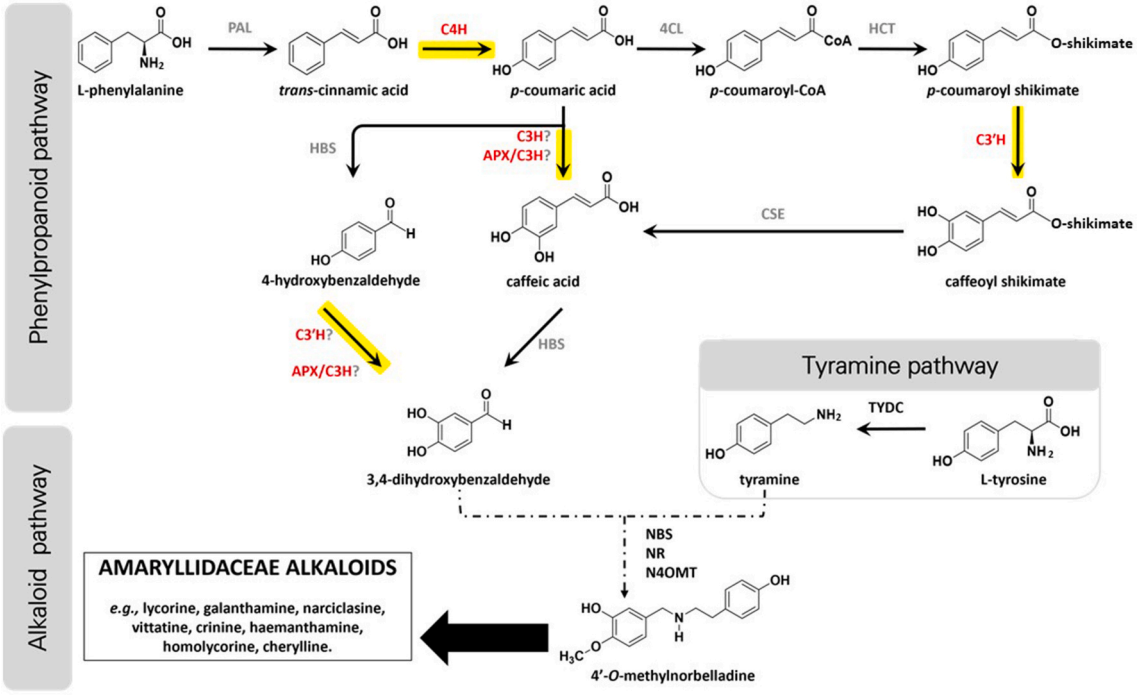


**Fig. 1.** The proposed pathway leading to 4′-*O*-methylnorbelladine, a common intermediate of Amaryllidaceae alkaloids. Enzymes shown in red were the primary enzymes studied in this work. Enzymes shown in black have been characterized in Amaryllidaceae, whereas enzymes in grey have not been characterized in Amaryllidaceae to date. Highlighted in yellow are the reactions investigated in this study. Abbreviations: PAL, phenylalanine ammonia-lyase; C4H, cinnamate 4-hydroxylase (CYP73A); 4CL, 4-coumarate:CoA ligase; HCT, hydroxycinnamoyl-CoA: shikimate hydroxycinnamoyl transferase; C3′H, *p*-coumaroyl shikimate/quinate hydroxylase (CYP98A); C3H, *p*-coumarate 3-hydroxylase (CYP98A); CSE, caffeoyl shikimate esterase; APX/C3H, ascorbate peroxidase/coumarate 3-hydroxylase; HBS, hydroxybenzaldehyde synthase; TYDC, tyrosine decarboxylase; NBS, norbelladine synthase; NR, noroxomaritidine/norcraugsodine reductase; N4′OMT, norbelladine 4′-*O*-methyltransferase.

## 2. Materials and methods

### 2.1. Plant materials and growth condition

The bulbs of *L. aestivum*, commonly known as summer snowflake, were bought from Vesey's (York, PE, Canada). The bulbs were grown outdoor in Trois-Rivières (Québec, Canada) until flowering. *N. benthamiana* seeds were germinated and grown indoors, in autoclaved AGRO MIX G6 potting soil (Fafard, Saint-Bonaventure, QC, Canada) with a long photoperiod (16 h light/8 h dark) at 22 °C.

### 2.2. Bioinformatic analysis, molecular homology modeling and docking

The open reading frames (ORF) and accession numbers were obtained from NCBI (ncbi.nlm.nih.gov). Molecular weight (MW) and isoelectric point (IP) were determined using Expasy (Duvaud et al., 2021). Sequence alignment utilized MegAlign Pro (DNASTAR, MegAlign Pro, version 17.4.1.17, Madison, WI: DNASTAR, Inc) and the Clustal Omega algorithm. MEGA11 was employed for Phylogenetic analysis with 1000 bootstrap replicates (Tamura et al., 2021). To visualize data, GraphPad Prism 8.0.1 (GraphPad Software, San Diego, California, USA) was utilized. Amino acid sequences corresponding to *Lae*C3′H and *Lae*C4H were uploaded onto the Protein Homology/analogY Recognition Engine V 2.0 (Phyre2) (Kelley et al., 2015) website, RosettaFold (Baek et al., 2021), and MOE 2020.09 software (Chemical Computing Group) for modeling the proteins. By comparing with crystalized orthologs (1PQ2 for human drug-metabolizing CYP450 2C8, 6VBY for cinnamate 4-hydroxylase (C4H) from *Sorghum. bicolor*) and Alphafold-predicted C4H from *Petunia hybrida* (AF-F1B282–F1-model_v4), the most consistent models were selected from Phyre predictions.

MOE was used to analyze the resulting homology model conformations, and to prepare receptors for docking, as described previously (Majhi et al., 2023). The structure preparation consisted of correcting issues, capping, charging termini, selecting appropriate alternate, and calculating optimal hydrogen position and charges using Protonate 3D. Energy minimization was performed for each fixed receptor with tethered active site that included positioned template substrates inside. Ready-to-dock substrates were uploaded from ZINC15 (Sterling and Irwin, 2015), or built from smiles codes with MOE builder. All protomers predicted at the enzymatic reaction pH were included as possible substrates. The MMFF94 × force field was used. Each receptor's active site was predicted using MOE Site Finder and used as docking site to place substrate using Triangle Matcher as placement method for 200 poses and tethered induced fit as refinement to perform flexible docking. Then, resulting poses were analyzed, and the best pose, according to comparison with a template's active site and to docking scores, was presented for each substrate. The protein-ligand interaction profiler (PLIP) was used to analyze the interactions between substrates and receptors' residues (Adasme et al., 2021), and the images were further processed using PyMOL (Shrödinger).

### 2.3. Yeast and bacteria growth conditions

*E. coli* DH5α (Invitrogen, Carlsbad, CA, USA) was cultured in Luria-Bertani (LB) medium with 50 μg.mL$^{-1}$ ampicillin at 180 rpm for 16 h at 37 °C. *Agrobacterium tumefaciens* GV3101 (Holsters et al., 1980) was grown in LB medium with kanamycin, rifampicin, and gentamicin (Fisher Scientific, ON, Canada) at 50, 50, and 30 μg mL$^{-1}$ final concentrations, respectively, with overnight incubation at 28 °C and 200 rpm stirring. *Saccharomyces cerevisiae*-derived yeast strain INVSc-1 (Invitrogen, Fisher Scientific) was grown in YPD complete media overnight at 30 °C with agitation at 200 rpm.

### 2.4. Chemicals

Caffeic acid (98%), ferulic acid (99%), and papaverine (98%) reference standards were purchased from Millipore Sigma (Massachusetts, USA). *p*-coumaric acid (98%), *trans*-cinnamic acid (98%), 4-hydroxybenzaldehyde, and 3,4-dihydroxybenzaldehyde (DHBA) reference standards were bought from Fisher Scientific (Ontario, Canada). *p*-coumaroyl shikimate and caffeoyl shikimate were chemically synthesized (Padmakshan et al., 2022). Analytical LC-MS grade methanol (99.9%) and formic acid (99%) were purchased from Fisher Scientific. Standard stock solutions of each reference standard were prepared at 100 mg. L$^{-1}$ in methanol and stored in the dark at −20 °C.

### 2.5. RNA extraction, cDNA synthesis, and differential expression analysis

One hundred and fifty mg of plant tissues, including bulb, root, stem, leaf, and flower of *L. aestivum* was ground in liquid nitrogen using a mortar and pestle and immediately transferred to a 1.5 mL Eppendorf tubes. Total RNA was extracted using TRIzol reagent (Invitrogen, Fisher scientific) according to the manufacture's instructions. After treatment with DNAse, quantification was done using Nanophotometer (Implen, Munich, Germany), and 1 μg of total RNA was used for cDNA synthesis using SensiFAST's cDNA synthesis kit (Bioline, London, England, United Kingdom) according to company's instructions, using both oligo(d)T and random hexamers.

Real-time quantitative PCR (RT-qPCR) was performed to investigate the expression pattern of the genes involved in Amaryllidaceae alkaloid and precursor pathway (Fig. 1 and Table A1) with Luna Universal qPCR Master Mix (New England Biolabs). The cycle program was set as: 95 °C for 2 min (1 cycle), [95 °C for 15 s, 60 °C for 30 s] (45 cycles)] followed by dissociation step 95 °C for 10 s, 50 °C for 5 s and 95 °C for 5 s *Histone 3* from *L. aestivum* was used as internal control. The threshold cycle (Ct) value of each gene was normalized against the Ct value of the reference gene. The relative gene expression levels were determined using the comparative ΔΔCt method (Pfaffl, 2001) by utilizing the average Ct values obtained from the technical triplicates. The obtained results were analyzed and visualized via CFX Maestro software (Bio-Rad).

### 2.6. Cloning, transformation procedure, and protein expression

Gene-specific forward and reverse primers (Table A1) were designed to isolate the coding sequences of *C4H*, *C3′H*, and *APX/C3H* from cDNA of *L. aestivum*. The open reading frames (ORFs) of *LaeC4H* and *LaeC3′H*, each in-frame with a Myc tag, were sequenced (Table A2) and cloned into the yeast expression vector pESC-LEU-*CroCPR*. Specifically, *LaeC4H* was inserted between *Apa*I and *Sal*I restriction sites, whereas *LaeC3′H* was inserted between *BamHI* and *Sal*I restriction sites. This vector already harbors the coding sequence of CYP450 reductase (CPR) from *Catharanthus roseus* (provided by Prof. Yang Qu at the University of New Brunswick). The ORF of *LaeAPX/C3H* was cloned in the bacterial expression vector pMAL-c2X (New England Biolabs) using *Bam*HI and *Sal*I restriction enzymes in frame with maltose-binding protein (MBP). Restriction enzymes were purchased from New England Biolabs. Using a heat-shock transformation method, all the constructs were delivered to chemically competent *E. coli* DH5α and selection was carried out on LB agar medium with ampicillin (50 μg .mL$^{-1}$). To isolate positive colonies, a colony PCR was performed using gene-specific primers and Taq DNA polymerase. The resulting plasmids were subjected to DNA sequencing to confirm the integrity of the target sequences.

The *S. cerevisiae* strain INVSc-1 was used for expressing recombinant *Lae*C4H and *Lae*C3′H proteins. Transformation with constructed vectors was performed using the Yeastmaker™ Yeast Transformation System 2 kit (Takara Bio). Positive yeast transformants were selected on yeast minimal leucine drop-out media. A single colony was precultured in 2 mL minimal leucine drop-out medium overnight at 30 °C, 200 rpm. This preculture was then inoculated into a 500 mL synthetic nitrogen base minimal medium lacking leucine with 5% glucose or dextrose (w/v) and incubated in the same condition. Yeast cells were collected, washed, and transferred to an induction medium (synthetic nitrogen base leucine

drop-out) with 10% galactose for 24 h in the same condition. Microsome preparation, adapted from (Pompon et al., 1996), involved resuspending cells in TES buffer (20 mM Tris-HCl [pH 7.5], 1 mM EDTA, 0.6 M sorbitol) and dividing into pre-chilled 1.5 mL tubes. The TES-yeast solution, containing 1 mm glass beads, was chilled, and cells were mechanically lysed using a TissueLyser (Qiagen, ON, Canada) at 30 Hz for 5 min (3 repetitions with cooling intervals). Lysed cells were centrifuged at 5000 rpm for 20 min at 4 °C, and the supernatant was subjected to ultra-centrifugation (Optima l-90 k, Beckman Coulter, ON, Canada) at 24,000 rpm for 60 min at 4 °C. The microsome pellet was resuspended in TEG buffer (50 mM Tris-HCl [pH 7.5], 1 mM EDTA, 20% v/v glycerol) and stored at −80 °C. The expression of recombinant proteins was verified using Western blot analysis.

To produce recombinant *Lae*APX/C3H, purified plasmids were transformed using heat shock transformation to chemically competent *E. coli* Rosetta (DE3) pLysS (Novagen) strain. Colony PCR was conducted to screen for positive transformants. Expression and purification steps of *Lae*APX/C3H followed as described in (Barros et al., 2019; Majhi et al., 2023). SDS-PAGE was performed to validate protein expression and purification.

### 2.7. In vitro enzymatic assay for LaeC4H, LaeC3′H and LaeAPX/C3H

The *in vitro* enzymatic assay for *Lae*C4H was performed according to (Ro et al., 2001), with a minor change in terms of incubation. Briefly, the reaction was adjusted to 600 μL total volume containing 50 μg microsomal fractions, NADPH (0.5 mM), sodium phosphate buffer (100 mM, [pH 7.4]), *trans*-cinnamic acid (0.1 mM), and incubated at 30 °C for 10, 30, 60, and 120 min, and overnight. The negative controls for the assays were: the reaction mixture with no NADPH, no substrate, no microsomal fractions, and microsomal fractions extracted from yeast harboring an empty vector. At the end of each time point, the reaction was terminated by adding 40 μL 6 M HCl. All reactions were performed in triplicate and each determination was repeated at least twice.

The activity of *Lae*C3′H was investigated as described previously (Schoch et al., 2001), with minor modification. Three different substrates, *p*-coumaroyl shikimate, free *p*-coumaric acid, and 4-hydroxybenzaldehyde (all at 0.1 mM final concentration) were tested in a 200 μL reaction containing 50 μg microsomal fractions, NADPH (0.6 mM), and sodium phosphate buffer (100 mM, [pH 7.4]). The samples were incubated at 28 °C for 30, 60, and 120 min, and overnight. The negative controls were the same as those described above. The reaction was terminated by adding 20 μL of acetic acid. All reactions were performed in triplicate and each determination was repeated at least twice.

The *in vitro* hydroxylase activity of *Lae*APX/C3H toward *p*-coumaric acid and 4-HBA was tested using the purified recombinant protein as previously described (Barros et al., 2019).

Following the reaction termination, papaverine (10 mg. $L^{-1}$ final concentration) was added to all the reactions, serving as an internal standard for the relative quantification of detected compounds. The reaction samples were mixed using a vortex, centrifuged 10 min at 12,000 rpm, and diluted 10-fold in mobile phase (formic acid 0.1% v/v in Milli-Q water and formic acid 0.1% v/v in methanol (90:10)). Analyses were conducted using HPLC-MS/MS as described below.

To determine the kinetic parameters of *Lae*C4H and *Lae*C3′H, enzymatic assays, as described in subsection 2.8, using a constant concentration of microsomal fractions while varying the concentration of respective substrates (in the case of *Lae*C3′H, only *p*-coumaroyl shikimate was used) ranging from 100 nM to 30 μM were carried out under the same conditions described above. The initial rate of reaction was measured for each substrate concentration. The maximum rate of reaction ($V_{max}$) and $K_m$ of the enzymes were determined using the Michaelis-Menten equation and non-linear regression analysis in GraphPad Prism 8.0.1.

### 2.8. Instrumentation and chromatographic conditions for enzymatic assays

A high-performance liquid chromatography (HPLC) system coupled with a tandem mass spectrometer (MS/MS) (Agilent Technologies, Santa Clara, California, USA) equipped with an Agilent Jet Stream ionization source, a binary pump, an autosampler and a column compartment were used for the analysis. Compounds separation was achieved using a Kinetex EVO C18 column (150 × 4.6 mm, 5 μm, 100 Å; Phenomenex, Torrance, USA). Five microliters of each sample were injected onto the column that was set at 30 °C. A gradient method made of (A) formic acid 0.1% v/v in Milli-Q water and (B) formic acid 0.1% v/v in methanol with a flow rate of 0.4 mL/min was used to achieve chromatographic separation. The HPLC elution program is described as follows: 0 min, 35% B; 10.0 min, 50% B; 16.0 min, 60% B; 16.2 min, 35% B. The total run time was 20 min per sample to allow the reconditioning of the column prior to the next injection. The parameters used in the MS/MS source were set as follows: gas flow rate 10 L. $min^{-1}$, gas temperature 300 °C, nebulizer 45 psi, sheath gas flow 11 L. $min^{-1}$, sheath gas temperature 300 °C, capillary voltage 4000 V in $ESI^+$ and 3500 V in $ESI^-$ and nozzle voltage 500 V. Agilent MassHunter Data Acquisition (version 1.2) was used to control the HPLC-MS/MS, and MassHunter Qualitative Analysis (version 10.0) was used for data processing.

### 2.9. Fusion fluorescent protein constructions, transient protein expression in N. benthamiana, and confocal microscopy

The open reading frame of *LaeC4H* and *LaeC3′H* genes were cloned into the *Kpn*I and *Xba*I sites of pBTEX binary vector in frame with yellow fluorescent protein (YFP) under the CaMV 35S promoter (Frederick et al., 1998). The resulted vectors, pBTEX-*LaeC4H-YFP* and pBTEX--*LaeC3′H-YFP*, were transformed to the *E. coli* DH5α chemical competent cells by the heat-shock method. The transformation mixtures were grown on LB agar medium with 50 μg $mL^{-1}$ kanamycin, and colony PCR was done to isolate positive colonies as described above. Each of the constructed vectors was transferred separately to *A. tumefaciens* strain GV3101 by electroporation and grown on LB agar containing kanamycin, rifampicin, and gentamicin, at the final concentration of 50, 50, and 30 μg $mL^{-1}$ respectively, and colony PCR was performed to select the positive transformants.

The transient expression in *N. benthamiana*, using *A. tumefaciens* bacteria was conducted as described previously (Majhi et al., 2023). To explore sub-cellular location of the *Lae*C4H and *Lae*C3′H, the leaves of 4-week-old *N. benthamiana* plants were co-infiltrated with *A. tumefaciens* harboring pBTEX-*LaeC4H-YFP* and *A. tumefaciens* containing either an ER marker (ER-mCherry) or a nuclear marker (Nls-CFP) in a 1:1 mixture. Forty-eight hours after co-infiltration, the fluorescent signals were visualized using Leica TCS SP8 confocal laser scanning microscope (Leica, Wetzlar, Hesse, Germany). The excitation and emission wavelength for YFP visualization were 488 and 500–525 nm, 405 and 420–490 nm for CFP, 587 and 610 nm for mCherry, whereas excitation and emission wavelengths to detect chlorophyll were set on 550 and 630–670 nm, respectively. The images were merged in Las X software (Leica 720 Microsystems).

### 2.10. Metabolite extraction and analysis

One gram of *L. aestivum* sample corresponding to the different plant part such as flower, stem, leaf, bulb, and root were ground under the liquid nitrogen by using a mortar and pestle. Crude metabolites extraction was performed by using 1 mL of methanol for 150 mg of plant tissue fresh weight. Extraction was carried out for 24 h at room temperature, followed by centrifuging at 10,000×*g* to remove plant debris. Samples were dried using speed vac concentrator and crude metabolite extract was reconstituted in methanol to have a final concentration of 1000 mg/mL and was filtered (0.2 μm Acrodisc® syringe filter, Pall

Corporation, NY). Target metabolite analysis was performed for phenylpropanoids and AAs. The LC-MS/MS method used is described in subsection 2.8 with some modification in the HPLC elution program which was set as follows: 0–10 min, 10% B; 20–25 min, 100% B; 26 min, 10% B. The total run time was 30 min per sample to allow the reconditioning of the column prior the next injection. Agilent MassHunter Data Acquisition (version 1.2) was used to control the HPLC-MS/MS, MassHunter Qualitative Analysis (version 10.0) and MassHunter Quantitative QQQ Analysis (version 10.0) were used for data processing. During extraction and metabolites analysis papaverine was used as internal standard. All the relative quantities of different metabolite were normalized with highest quantity in each tissue type and visualized by using Graph pad Prism 8.0.1.

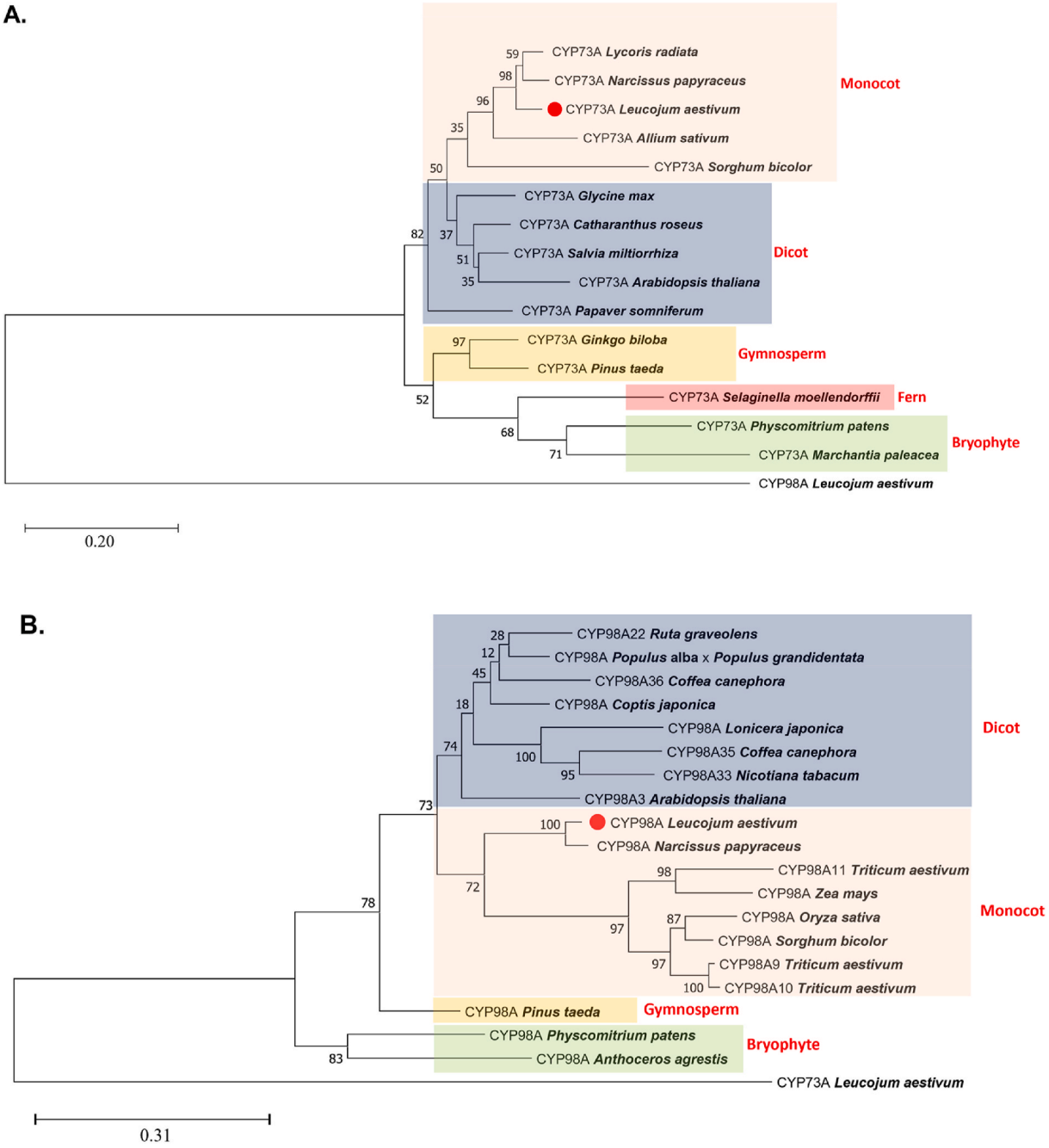


**Fig. 2.** Phylogenetic tree of *L. aestivum* enzymes indicated with circles (●). The analysis was performed using the Maximum Likelihood method with 1000 bootstrap replicates with the Mega11 software for **A.** *Lae*C4H of species *L. radiata* (AWW24970), *N. papyraceus* (AXU39895), *L. aestivum* (UIP35210), *Allium sativum* (ADO24190), *S. bicolor* (AAK54447), *Glycine max* (ACR44227), *C. roseus* (CAA83552), *Salvia miltiorrhiza* (ABC75596), *A. thaliana* (AAC99993), *Papaver somniferum* (XP_026,426,522), *G. biloba* (AAW70021), *Pinus taeda* (AAD23378), *S. moellendorffii* (EFJ22128), *P. patens* (ADF28535), *M. paleacea* (ASA39648). The CYP98A (UIP35212) from *L. aestivum* was used as an outgroup; **B.** *Lae*C3′H with species *Ruta graveolens* (AEG19446), *Populus alba* × *Populus grandidentata* (ABY85195), *Coffea canephora* (ABB83676, ABB83677), *Coptis japonica* var. Dissecta (BAF98473), *Lonicera japonica* (AGQ48118), *Nicotiana tabacum* (ABC69384), *A. thaliana* (NP 850337), *L. aestivum* (UIP35212), *N. papyraceus* (AXU39897), *Triticum aestivum* (CAE47491, CAE47489, CAE47490), *Zea mays* (PWZ32976), *Oryza sativa* (AAU44038), *S. bicolor* (XP_002,440,001), *P. taeda* (AAL47685), *P. patens* (XP_024,360,823), *Anthocero agrestis* (QPI70542), and CYP73A (UIP35210) from *L. aestivum* was used as an outgroup. The bootstrap values are indicated at the branch-points.

### 2.11. In vivo enzymatic assay of LaeC4H and LaeC3′H

*Lae*C4H and *Lae*C3′H were transiently expressed in *N. benthamiana* leaves, as described in subsection 2.8, to evaluate the impact of the overexpressed enzymes on phenolic compound levels *in planta*. A vector expressing yellow fluorescent protein (YFP) was used as negative control. Subsequently, 2 days post-agroinfiltration, leaves were treated with 100 μM of substrates and then incubated under the same conditions. After 24 h, four leaves from each plant were harvested, pooled, and ground with liquid nitrogen for storage at −80 °C until analysis. Metabolite extraction and analysis were conducted using 100 mg of each sample as describe in subsection 2.10 with a minor modification. A second analysis was performed in duplicate following a 10-fold concentration of metabolite before injecting in HPLC-MS/MS.

## 3. Results

### 3.1. Identification and sequence analysis of LaeC4H and LaeC3′H from L. aestivum

The full-length open reading frame (ORF) sequences of predicted *LaeC4H* (505 amino acids (aa)) and *LaeC3′H* (509 aa), and *LaeAPX/C3H* (248 aa) were extracted from *L. aestivum* transcriptome (Tousignant et al., 2022). The NCBI accession numbers are as follows: UIP35210 (*LaeC4H*), UIP35212 (*LaeC3′H*), and MW971972.1 (*LaeAPX/C3H*) (Table A2). Predicted hypothetical molecular weights (MW) and isoelectric points (IP) for these proteins are as follows: *Lae*C4H (57.97 kDa, 9.12), *Lae*C3′H (57.8 kDa, 8.6), and *Lae*APX/C3H (5.84 kDa, 27.2). Multiple sequence alignments were performed for *Lae*C4H and *Lae*C3′H, separately, with homologous sequences selected from monocot, dicot, gymnosperm, pteridophyte, and bryophyte species. *Lae*C4H shared a high amino acid sequence identity of 94.5% with Amaryllidaceae *Lycoris radiata*. Substantial identity was also observed with counterparts from various plant groups, including monocots (78% to *S. bicolor*), dicots (84% to *A. thaliana* and 85% to *C. roseus*), gymnosperms (80% to *Ginkgo biloba*), and a fern, *Selaginella moellendorffii*, with 80% identity (Fig. 2A and Fig. A1). Lower but still high levels of identity were noted between *Lae*C4H and *Marchantia paleacea* (65%) and *Physcomitrella patens* (70%), as representatives of bryophytes. *Lae*C3′H shared a high level of identity (95%) with the predicted homologue in *Narcissus papyraceus*. Compared to *Lae*C4H, *Lae*C3′H was more distantly related to other homologues, such as monocot *Sbi*C3′H (71%), dicot *Ath*C3′H (73%), gymnosperm *Pta*C3′H (73%), and bryophyte *Ppa*C3′H (64%) sequences (Fig. 2B and A2). *Lae*C4H and *Lae*C3′H and their Amaryllidaceae paralogs formed a clade with monocot species, adjacent to the dicot clade, but further from gymnosperm, pteridophyte, and bryophyte homologues (Fig. 2B).

*Lae*C4H and *Lae*C3′H belong to the CYP73A and CYP98A enzyme families, respectively. As CYP450, they share multiple domains, such as a common N-terminal membrane-anchoring domain that enables binding to the cytoplasmic surface of the endoplasmic reticulum membrane (Nelson and Strobel, 1988; Li et al., 2016). Using multiple sequence alignment, we identified the characteristic membrane-anchoring domain in *Lae*C4H (Fig. A1), which appeared to be highly conserved among the C4Hs from monocot and dicot plants, but less so within other plant groups such as bryophytes. By contrast, for *Lae*C3′H, no conserved pattern was observed in the membrane binding domain region of C3′H homologues (Fig. A2). The proline-rich motif (PPGPLPV) is another conserved signature of CYP450 that is hypothesized to be involved in the folding and proper integration of heme and the stability of microsomal proteins that was observed in both enzymes (Figs. A1 and A2) (Li et al., 2016; Szczesnaskorupa et al., 1993; Teutsch et al., 1993). The helix I motif (AAIET including conserved Ala306 and Ala 307) speculated to play a role in proton transfer and oxygen activation, was conserved in all aligned C4H sequences, including *Lae*C4H (Fig. A1) (Sen and Thiel, 2014). Similarly, a proposed oxygen binding motif (AGMDT) (Kriegshauser et al., 2021) was found to be conserved among C3′H homologues. The heme-binding domain (FGVGRRSCPG in C4H and FGAGRRVCPG in C3′H) is a key feature of CYP450 superfamily, which was indeed preserved in both *Lae*C4H and *Lae*C3′H along with other plant species (Figs. A1 and A2). This segment encompasses the cysteine pocket enclosing the heme and interaction with Cys 447-S in a hydrophobic environment.

### 3.2. Prediction of substrate interaction for LaeC4H and LaeC3′H

*Lae*C4H and *Lae*C3′H structures and active sites were modelled to gain further understanding of their activity. *Lae*C4H and *Lae*C3′H were structurally similar, visible as an α-helix-rich triangular shape, like other CYP450s (Fig. 3A and B, and Fig. A3, Table A4). The active site in both enzymes formed a large canal crossing the enzyme. The heme pocket was deeply buried within the protein large cavity, and two lobes extended from this stem on both sides (Fig. 3A and B, Table A3). The left side lobe lined by the F and G α-helices is speculated to be the substrate entry port (Fig. A3) (Zhang et al., 2020). The disparity between *Lae*C3′H and *Lae*C4H in the sequences of the A, F and G helices and the connecting loop with B′ α-helix likely may confer unique specificity onto each CYP450 enzyme towards various substrates. The right extension was longer in the *Lae*C3′H predicted structure, possibly allowing binding of larger substrates. Molecular docking was used to study the orientation, affinity, and interaction of putative phenylpropanoid substrates with *Lae*C4H and *Lae*C3′H. The interactions between *trans*-cinnamic acid and *Lae*C4H were mapped based on a comparison with similar enzymes in other plant species (Fig. 3C and Table A4). HEPES was first docked into *Lae*C4H to validate our model by comparison with previously crystalized structures. It docked in an axial position on the *Lae*C4H active site with a score of −7.32 kcal $mol^{-1}$ in a position analogous to HEPES in the crystalized structure of *Sb*C4H (PDB: 6VQY), reflecting the affinity of the enzyme for this substrate (Zhang et al., 2020) (Fig. A4). *Trans*-cinnamic acid docked with a score of −5.12 kcal $mol^{-1}$ (Fig. 3C). The smaller atomic size of this ligand compared to HEPES could be reflected in a smaller score (Plewczynski et al., 2011). Nonetheless, it positioned itself similarly at the stem, on the distal side of the heme, opposite to the axial thiolate, stabilized by hydrophobic interactions with Val 118, Phe 119, Val 305, Ala306, Val 375, and Phe 488 with its phenylpropene portion, as well as an H-bond between Gln 218 located in the F helix and the O at the carboxyl group of the substrate (Fig. 3C). Positioning and detected interactions were similar to those in a previous study on *Sbi*C4H (Zhang et al., 2020). The substrate phenol ring C4 was at 4.2 Å of the heme, a positioning that is consistent with the ferrous ion being ligated to the molecular oxygen yielding hydroxylation of this atom to obtain *p*-coumaric acid.

The interactions between *p*-coumaric acid, 4-HBA, or *p*-coumaroyl shikimate substrates and the active site of *Lae*C3′H was also studied (Fig. 3D, E and F). These bulkier ligands were included as possible substrates to clarify the controversy surrounding the catalytic activity of *Lae*C3′H, probing the compatibility with its active site. *p*-Coumaric acid, 4-HBA, and *p*-coumaroyl shikimate docked with a score of −5.52, −4.67 and −7.04 kcal/mol, respectively (Table A4). Upon docking, substrates oriented analogously to that of *p*-coumaroyl shikimate with wheat CYP98A10 and CYP98A11 (Morant et al., 2007), *i.e.,* their phenylpropanoid moiety close to the heme center in a bent conformation, aromatic carbon C3 oriented toward the heme at a distance of 3.7 (*p*-coumaroyl shikimate), 3.9 (*p*-coumaric acid) and 4.1 Å (4-HBA) (Fig. 3D, E, and F). For all substrates, the propylbenzene group was stabilized by: 1) hydrophobic interactions with Ala300, and Leu369, and 2) hydrogen bonds with Thr304 and Thr365. Trp 114 formed a hydrogen bond with the carbonyl group of all three substrates. *p*-Coumaric acid interacted with the active site through additional hydrophobic bonds with Ile 113 and Thr365; Ala300, Thr304 and Leu369 participated in both substrate interaction stabilization through hydrophobic bonding, and stabilization of the heme. A hydrogen bond with Leu 215 and a salt bridge with Lys216 stabilized the shikimate portion of *p*-coumaroyl

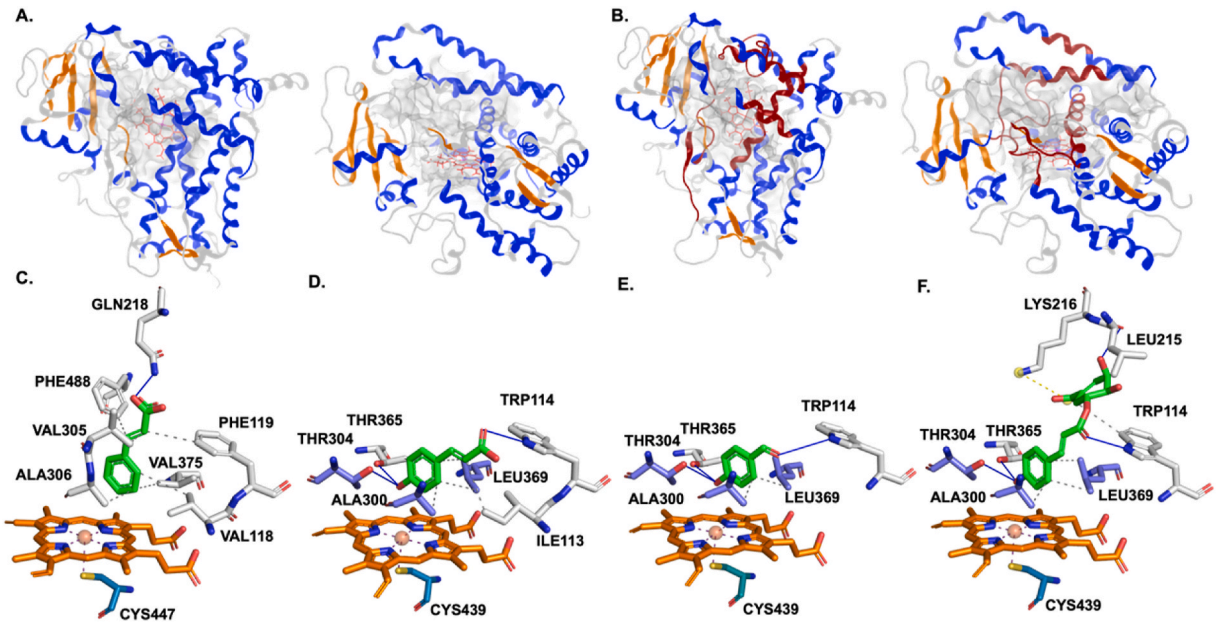


**Fig. 3.** Representation of *Lae*C4H and *Lae*C3′H structures. **A.** Cartoon representation of *Lae*C4H with grey transparent surface-active site, top of the heme view (left) and perpendicular side of the heme plan (right). **B.** Cartoon representation of *Lae*C3′H with grey transparent surface-active site, top of the heme (left) and perpendicular side of the heme plan (right). Heme group is shown as red sticks. Conserved α-helix (blue) and β-strands (orange) secondary structures are shown. Conserved CYP98A substrate recognition is displayed in red. **C.** *trans*-Cinnamic acid (green) interactions with *Lae*C4H residues at its active site; **D**, **E,** and **F.** Interactions of *p*-coumaric acid (green), 4-hydroxybenzaldehyde (green), and *p*-coumaroyl shikimate (green) with *Lae*C3′H at its active site. Residues are shown as sticks. The heme group is orange, grey residues interact with substrates only, purple/violet residues interact with both heme and substrate. H-bonds are shown as blue lines, hydrophobic interactions as dashed green lines, and salt bridges as dashed yellow lines.

shikimate (Fig. 3F). Potential electron donors and acceptors were present in the site interacting with all substrates and orientation of each docked substrate appeared to be favorable for its *m*-hydroxylation. *p*-Coumaric acid and 4-HBA docking scores were lower, with fewer H-bonds and no salt-bridge between the active site residues and the substrates (Table A4), and a higher distance to the heme, compared to *p*-coumaroyl shikimate. Altogether, these results suggest that *p*-coumaroyl shikimate is the most suitable substrate for *Lae*C3′H.

### 3.3. Recombinant protein expression in yeast and bacterial host, and in vitro enzymatic assays

CYP450 enzymes are commonly known to be localized to the ER membrane by an N-terminal hydrophobic anchor, which is necessary for their optimal functionality. A eukaryotic, yeast expression system was therefore selected to provide canonical localization. CYP450s were cloned into vectors containing the requisite redox partner, a CYP450 reductase from *C. roseus* (*Cro*CPR). Microsomal fractions were isolated from strains expressing either *Lae*C4H-Myc or *Lae*C3′H-Myc recombinant proteins. Expression was confirmed by SDS-PAGE and Western blot analysis, which revealed the expected bands (Fig. A5).

The microsomal fractions were subjected to *in vitro* enzymatic assay. *Lae*C4H microsomal fractions were supplemented with *trans*-cinnamic acid, and the reaction mixture was incubated for 10 and 30 min, 1 and 2 h, and overnight at 30 °C. Representative results corresponding to 30 min incubation time are shown (Fig. 4A). The reaction product, *p*-coumaric acid, was detected at all incubation periods above 10 min (Fig. A6). Thus, the results showed that C4H from *L. aestivum* can efficiently hydroxylate *trans*-cinnamic acid to produce *p*-coumaric acid.

Similarly, recombinant *Lae*C3′H-Myc was tested with various substrates, including *p*-coumaroyl shikimate, identified as the most probable substrate, free *p*-coumaric acid, and 4-HBA. The reaction mixtures were subjected to HPLC-MS/MS analysis. A signal corresponding to caffeoyl shikimate in the test tube supplemented with *p*-coumaroyl shikimate was detected at all time points (Fig. 4B and Fig. A7). In contrast, no reaction product, including no signal for caffeic acid or DHBA, were detected when *p*-coumaric acid or 4-hydroxybenzaldehyde were used as substrates.

The kinetic parameters of *Lae*C4H and *Lae*C3′H were determined using enzymatic assays. Microsome fractions were maintained at a constant concentration, while the concentration of the respective substrates varied from 100 nM to 30 μM (Fig. A8). The maximum rate of reaction (Vmax) and Km of the enzymes were determined using Michaelis-Menten equation and non-linear regression analysis (Table 1). *Lae*C4H ($K_m$ 3.32 μM; $V_{max}$ 0.17 μM/min) show higher affinity and speed of catalysis toward its substrate, than *Lae*C3′H ($K_m$ 22.16 μM; $V_{max}$ 5.89 μM $min^{-1}$).

*Lae*APX/C3H was expressed in bacterial system and validated using SDS-PAGE (Fig. A9). Enzymatic activity of *Lae*APX/C3H was performed using *p*-coumaric acid and 4-HBA to assess 3-hydroxylation. A reaction mixture without *Lae*APX/C3H was used as negative control. Caffeic acid was detected in the enzymatic reaction supplemented with *p*-coumaric acid; however, the amount of caffeic acid was higher in the negative control (Figs. A10 and A11). Using increasing amount of enzyme in the reaction, *p*-coumaric acid progressively disappeared, but caffeic acid level did not rise above the level of the negative control (Fig. A11). This suggested that the enzyme consumed *p*-coumaric acid, but caffeic acid was not the corresponding product. This result is consistent with the study of (Zhang et al., 2023b) reporting that the caffeic acid level in the reaction without and with a homologous APX/C3H from monocot *S. bicolor* was not significantly different. DHBA was detected in both enzymatic reaction and in the negative control with 4-HBA as a substrate. No significant changes were observed in 4-HBA consumption by increasing the enzyme concentration, suggesting that the enzyme did not accept 4-HBA as a substrate (Fig. A11).

### 3.4. Subcellular localization of LaeC4H and LaeC3′H in N. benthamiana

C-terminal YFP-fusion *Lae*C4H and *Lae*C3′H were co-expressed with an endoplasmic reticulum marker (ER-mCherry) and a nucleus marker

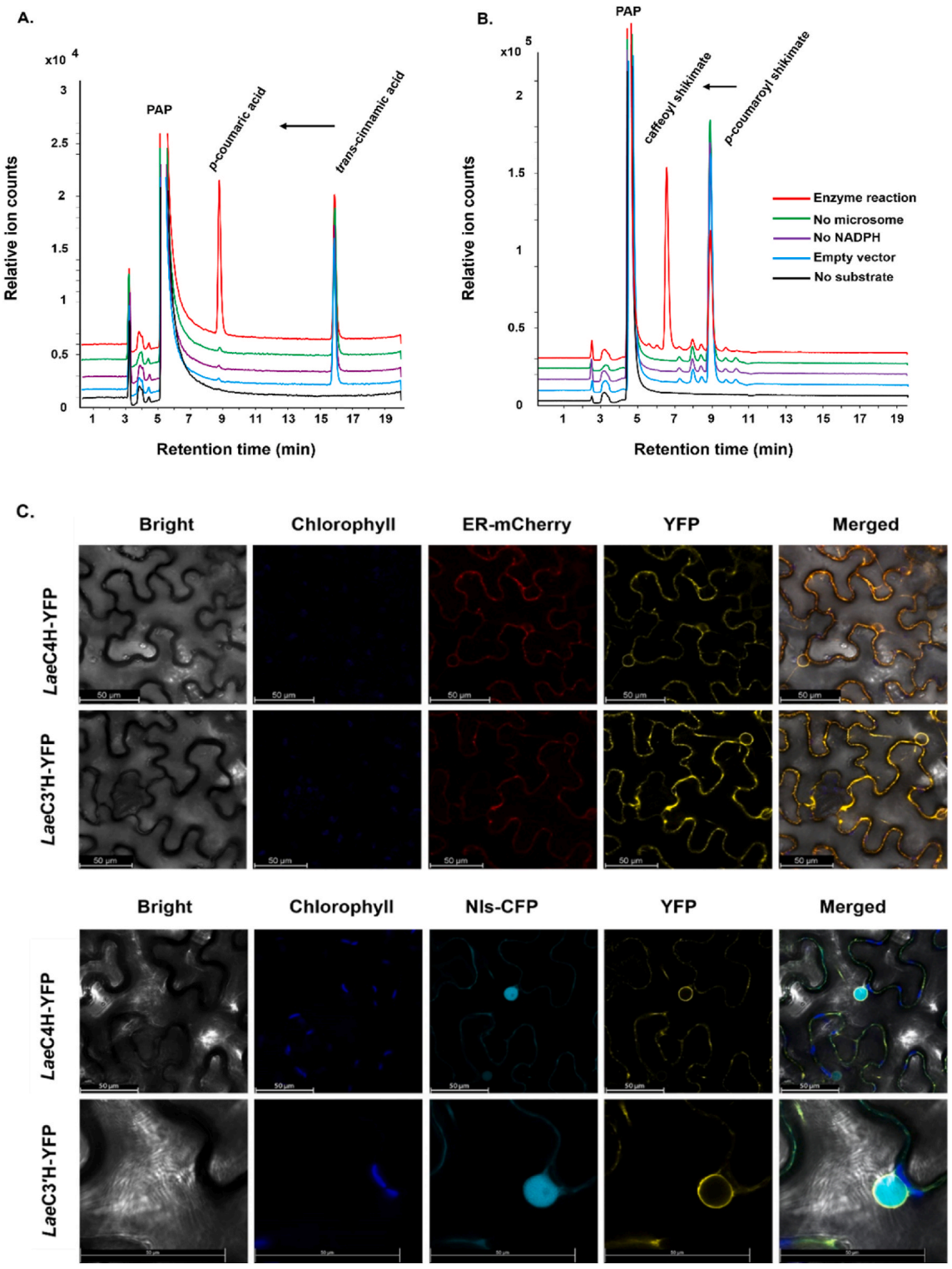


**Fig. 4.** HPLC-MS/MS analysis of representative enzymatic assay for *Lae*C4H (A) and *Lae*C3′H (B), and their subcellular localization in *N. benthamiana* (C). **A.** *trans*-Cinnamic acid was tested on microsome fractions extracted from yeast harboring the *Lae*C4H-Myc construct, and *p*-coumaric acid (red) formation was detected; **B.** Assays with microsomes containing *Lae*C3′H-Myc using *p*-coumaroyl shikimate, and the samples were subjected to the detection of caffeoyl shikimate. Red, peaks resulting from the sample containing microsomal recombinant proteins (*Lae*C4H-Myc and *Lae*C3′H-Myc); Purple, peaks from the sample without NADPH; Blue, peaks from the sample containing empty vector microsomal fractions; Green, peaks from the sample without recombinant protein; and black represents the peak from the sample without substrate. Papaverine (PAP) was used as a standard control; **C.** Subcellular localization of *Lae*C4H and *Lae*C3′H in *N. benthamiana* epidermal leaf. Fusion fluorescent proteins were co-expressed with ER marker (ER-mCherry) (upper panel), and nucleus marker (Nls-CFP) (bottom panel) in *N. benthamiana* leaves by the *Agrobacterium*-mediated transient expression method, and subsequently the fluorescent signals were detected by confocal microscopy 48 h after co-infiltration. The scale bars in the pictures indicate 50 μm.

**Table 1**
Kinetic parameters for *Lae*C4H and *Lae*C3′H.

| Enzyme | $V_{max}$ (μM.min$^{-1}$) | $K_m$ (μM) |
|---|---|---|
| *Lae*C4H | 0.12 | 1.21 |
| *Lae*C3′H | 5.89 | 22.16 |

(Nls-CFP) in *N. benthamina* leaf using agroinfiltration to explore their subcellular localization. As expected, *Lae*C4H and *Lae*C3′H colocalized to the ER (Fig. 4C, upper panel), which is consistent with previously reported cellular localizations for both enzymes from other species. Co-expression with a nucleus marker indicated that the target proteins are not localized inside the nucleus. Yellow fluorescence was observed in the vicinity of the nuclear membrane that would suggest localization of both enzymes in the membrane region closely associated with the nuclear envelope (Fig. 4C, bottom panel). The integrity of the expressed fusion proteins was validated by Western blot analysis using an anti-YFP primary antibody (Fig. A12).

### 3.5. *In vivo* enxymatic assay of *LaeC4H and LaeC3′H*

*Lae*C4H and *Lae*C3′H were transiently expressed, and their respective substrates were fed to *N. benthamiana* leaves to confirm their functionality *in planta.* Unexpectedly, upon expression of *Lae*C4H and feeding with *trans*-cinnamic acid, *p*-coumaric acid was not detected, but *p*-coumaroyl shikimate was observed (Fig. 5 and Table A5). This suggested that *Lae*C4H expression yielded *p*-coumaric acid from *trans*-cinnamic acid, but the latter was rapidly converted to *p*-coumaroyl shikimate by endogenous enzymes (Fig. 1). Interestingly, caffeoyl shikimate, produced by the endogenous C3′H, was also detectable in these plants. To gain further precision, samples were concentrated 10 times, revealing that plants infiltrated with *Lae*C4H and *trans*-cinnamic acid had increased production of three downstream products, *i.e. p*-coumaroyl shikimate, caffeoyl shikimate, and caffeic acid. In corresponding controls, these compounds were not detected. In plants overexpressing *Lae*C3′H and fed with *p*-coumaroyl shikimate, caffeoyl shikimate, the direct product of this enzyme, was detectable as well, whereas plants fed with *p*-coumaroyl shikimate without *Lae*C3′H demonstrated no detectable level of caffeoyl shikimate. Additionally, caffeic acid, a downstream product of these enzymes, also accumulated to detectable levels in plants overexpressing the enzymes, providing indirect evidence for the activity of *LaeC4H* and *LaeC3′H in planta* (Fig. 5 and Table A5).

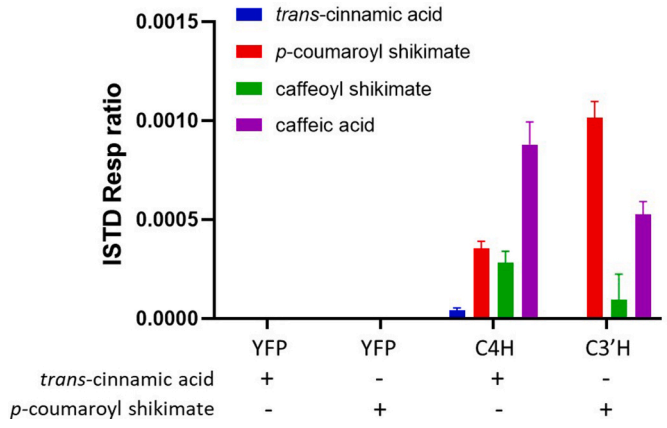


**Fig. 5. *In vivo* enzymatic activity of *LaeC4H* and *LaeC3′H*.** Metabolite extracts from samples listed in Table A5 were concentrated and analyzed using HPLC-MS/MS. Control samples included: 1) plants without infiltration and feeding to distinguish the level of endogenous phenolic compounds from those altered by experimental conditions, 2) plants expressing the YFP, and 3) YFP-expressing plants fed with the substrates to assess the non-specific effect of *Agrobacterium* infection on phenolic compounds. NA: not applicable. This experiment was performed in biological duplicates of 5 leaves-pooled samples.

### 3.6. *Metabolite profiling of L. aestivum plant organs*

Targeted LC-MS/MS analyses of metabolite extracts from different parts of *L. aestivum* were performed to identify and measure relative metabolite levels for intermediates of AA biosynthesis (Fig. 6A).

Tyrosine, and phenylalanine were detected at higher levels in bulb and flower tissues (Fig. 6A). Tyramine was detected in bulb and flower tissues, but mostly accumulated in the roots (2-fold increase compared to bulb). *p*-Coumaric acid, caffeic acid, and ferulic acid were detected only in the flowers. In general, AAs were detected in several tissues, and in higher quantities in the bulbs and flowers compared to other tissues. Specifically, lycorine accumulated almost 4- and 2-fold more in bulbs and flowers as compared to leaves and roots respectively. Norgalanthamine, vittatine and 11-hydoxyvittatine were more abundant in the flower as compared to other parts of *L. aestivum*. Interestingly, flowers were the only tissues to concurrently accumulate all the tested precursor metabolites and intermediates of AA biosynthesis.

### 3.7. *Differential expression analysis*

Both C3′H and C4H are key enzymes of the phenylpropanoid pathway. Their differential expression together with transcript levels of genes encoding enzymes involved in the biosynthesis of AA precursors and end-products was explored in different plant tissues of *L. aestivum* (Fig. 6B). RT-qPCR analysis showed that transcripts involved in the phenylpropanoid pathway were expressed higher in roots as compared to other parts of the plant. *PAL*, *C4H*, *C3′H*, and *TYDC1* were all expressed at significantly higher levels in roots (Fig. 1). Relatively higher expression of *TYDC2* and *C3′H* along with other AA-specific genes including *NBS*, *NR,* and *N4′OMT* (Fig. 6B) in alkaloid containing tissues could highlight their potential role in providing the intermediates to AA biosynthesis. The high abundance of tyramine in roots was consistent with increased transcript levels of *TYDC1* compared to other tissues. Unlike *TYDC1, TYDC2* was mostly expressed in leaves and stem unrelated to the tyramine content of those tissues.

## 4. Discussion

Amaryllidaceae plants accumulate specialized metabolites such as specific alkaloids known for their therapeutic potential. Their production is controlled by the enzymes involved in their biosynthesis and in the phenylpropanoids formation, through a complex process. The phenylpropanoid pathway also catalyzes the formation of the precursors of lignin, lignans, flavonoids. The biosynthesis of the AA precursor DHBA starts with phenylalanine and requires two hydroxylation reactions (Desgagné-Penix, 2021). C4H was shown to introduce the first hydroxyl group at the 4-position of the aromatic ring of *trans*-cinnamic acid in several plant species (Li et al., 2018c) (Fig. 1). The enzyme responsible for the 3-hydroxylation remained uncharacterized for a long time, but in recent years, C3′H (CYP98) was proposed as the major 3-hydroxylase in the phenylpropanoid pathway in *A. thaliana* (Schoch et al., 2001). Other studies suggested that it was rather catalyzed by APX/C3H in *Brachypodium distachyon* (Barros et al., 2019) but not in *Sorghum bicolor* (Zhang et al., 2023a). In the current study, a survey of the transcriptome data of *L. aestivum* (Tousignant et al., 2022) allowed the identification of putative *Lae*C4H, *Lae*APX/C3H and *Lae*C3′H genes.

The *Lae*C4H sequence was highly similar to those of other monocot C4Hs with distinctive conserved domains and active residues. This suggests a very low level of evolutionary pressure during the diversification of the land plants. In the predicted model of *Lae*C4H, *trans*-cinnamic acid was docked in a position consistent with its 4-hydroxylation, yielding *p*-coumaric acid, as observed in previous reports (Chen et al., 2011; Li et al., 2018a, 2018b, 2020). We further confirmed that microsomes extracted from *Lae*C4H-transformed yeast catalyze the

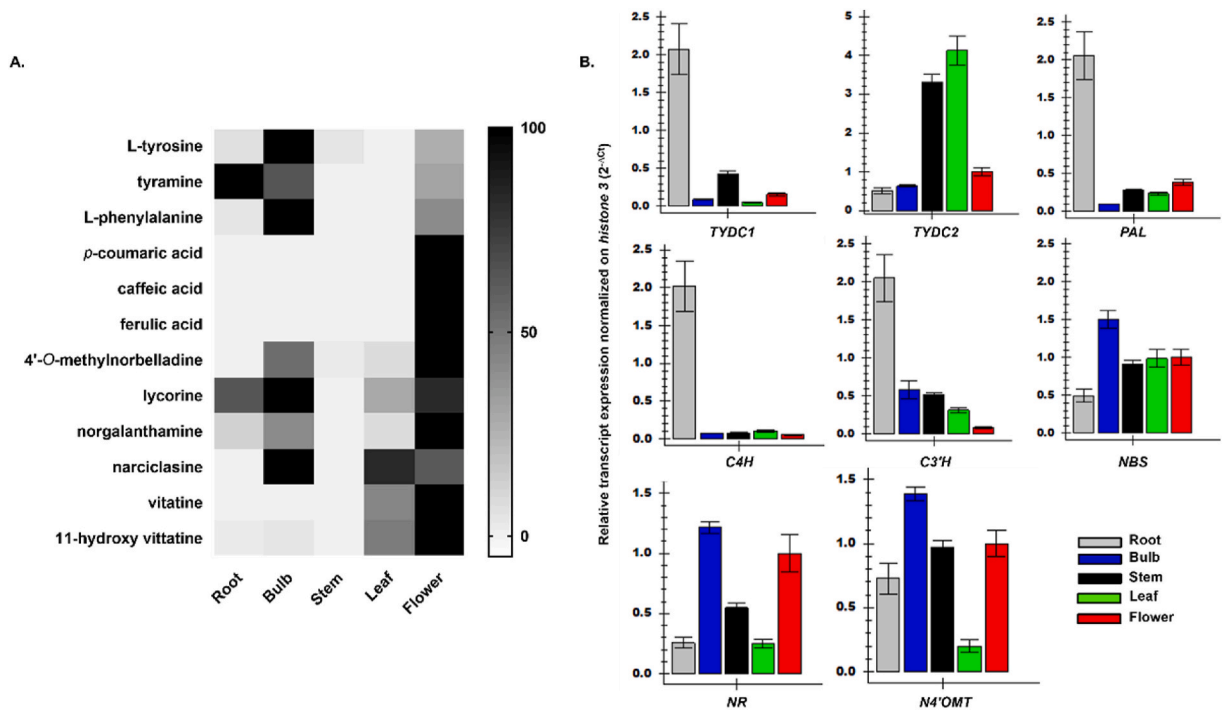


**Fig. 6.** Metabolic profile and expression analyses. **A.** Targeted metabolite profiling from different tissues of *L. aestivum.* Heat Map showing the relative abundance of Amaryllidaceae alkaloids (precursors, intermediates, and end products) from different part of *L. aestivum*. Relative abundance corresponds to the mean value of three independent replicates. Values were normalized to the sample with the highest level for each compound in different tissues; **B.** qRT-PCR analyses of precursor and AAs specific genes from different plant tissues of *L. aestivum* including bulb, flower, leaf, root, and stem. The genes include *phenylalanine ammonia lyase* (*PAL*), *tyrosine decarboxylase* (*TYDC1*, *TYDC2*), *C4H*, *C3′H*, and several AA-specific genes such as *norbelladine synthase* (*NBS*), *noroxomaritidine/norcraugsodine reductase* (*NR*) and *norbelladine 4-O-methyltransferase* (*N4′OMT*). Three biological and two technical replicates were performed for each gene.

4-hydroxylation of *trans*-cinnamic acid *in vitro*. The $K_m$ value for *Lae*C4H towards cinnamic acid was consistent with values reported elsewhere (Liu et al., 2017), supporting *trans*-cinnamic acid as the C4H substrate. Previous work on the heterologous expression of truncated Amaryllidaceae C4H from *L. aurea* and *L. radiata* in bacteria showed that the enzyme was functional without its N-terminal membrane domain (Li et al., 2018a, 2018b). However, the latter mediates the anchoring to the exterior surface of the ER (Werck-Reichhart and Feyereisen, 2000) and ensures the correct sub-cellular localization. This localization facilitates interactions with the electron donor reductase partner and other pathway enzymes (Hansen et al., 2021), potentially promoting the formation of a metabolon for efficient metabolite channeling (Achnine et al., 2004).

The *Lae*C3′H sequence was also similar to those of monocot, although a little more distant compared to *Lae*C4H. Evolutionary analysis of the C3′H family has been discussed by Alber et al. (2019), reporting that they had a single origin in a common ancestor of all land plants. The study highlighted multiple gene duplications within angiosperms, leading to small clusters of gene families in most species. Previous studies revealed a wide range of possible substrates for C3′H. In dicot and monocot angiosperms, *p*-coumaroyl shikimate has been reported to be the preferred substrate for CYP98A enzyme family (Alber et al., 2019). In *A. thaliana*, C3′H (CYP98A3) also catalyzed 3′-hydroxylation of *p*-coumaroyl quinate (Schoch et al., 2001), whereas C3′H (CYP98A8 and CYP98A9) showed 3′-hydroxylase activity toward spermidine-conjugated phenolics (Matsuno et al., 2009), and naringenin (in the case of CYP98A9) (Liu et al., 2016). In wheat, a CYP98A12 isoform could hydroxylate *p*-coumaroyl tyramine to caffeoyl tyramine that was subsequently methylated to feruloyl tyramine as part of a pathogen-induced defense response (Morant et al., 2007). Considering the substrate promiscuity of C3′H in different plant groups, we hypothesized that *L. aestivum* C3′H was capable of hydroxylating 4-HBA along with previously reported substrates like *p*-coumaroyl shikimate and, free *p*-coumaric acid. Modelled structure and docking analysis suggested that *Lae*C3′H pocket was more consistent with 3-hydroxylation of large substrate such as *p*-coumaroyl shikimate stabilized by key additional hydrophobic interactions, H-bonds and a salt bridge with Lys216 with the shikimate portion, compared to HBA or *p*-coumaric acid. This was confirmed by *in vitro* enzymatic assay yielding caffeoyl shikimate from *p*-coumaroyl shikimate, whereas other substrates were not hydroxylated by C3′H. Thus, *Lae*C3′H does not catalyze the synthesis of caffeic acid or DHBA.

Recently, it has been proposed that direct hydroxylation of free *p*-coumaric acid is rather catalyzed by a bifunctional ascorbate peroxidase/4-coumarate 3-hydroxylase, a non-membrane enzyme purified from different plant species (Barros et al., 2019). We identified and cloned a homologous *Lae*APX/C3H and successfully expressed it in a prokaryotic system. *Lae*APX/C3H did not catalyze the 3-hydroxylation of HBA or *p*-coumaric acid. Although caffeic acid was detected when *p*-coumaric acid was used as a substrate, it was more abundant in the reaction mixture lacking *Lae*APX/C3H, showing that its production was not enzyme dependent. A progressive consumption of *p*-coumaric acid was detected with increased concentration of enzymes, implying that this enzyme consumes *p*-coumaric acid, possibly for polymerization, as evidenced in *S. bicolor* (Zhang et al., 2023b).

To confirm the activity of *Lae*C4H and *Lae*C3′H *in planta*, the enzymes were expressed, and their substrates were fed in *N. benthamiana* leaves. Infiltration with *Lae*C4H and feeding with *trans*-cinnamic acid led to the specific detection of *p*-coumaroyl shikimate, caffeoyl shikimate, and caffeic acid, while *Lae*C3′H combined to *p*-coumaroyl yielded caffeoyl shikimate and caffeic acid. Unexpectedly, *p*-coumaric acid, the direct product of *Lae*C4H was not detected. We hypothesized that *p*-coumaric acid was converted to the detected downstream products by endogenous enzymes such as 4CL and HCT (Fig. 1). In various plant species, *p*-coumaric acid can rapidly be metabolized to *p*-coumaroyl CoA, serving as a pivotal entry point for various metabolic pathways, including the

biosynthesis of flavonoids, stilbenes, coumarins, monolignols of lignin, among others. Many of these compounds trigger defense mechanisms against wounds and external infections (Uhlmann and Ebel, 1993; Hu et al., 2010). Overall, these results provide *in planta* evidence of the functionality of *Lae*C4H and *Lae*C3′H.

In summary, we showed that C4H catalyzes the production of *p*-coumaric acid, which can be converted to *p*-coumaroyl-CoA and *p*-coumaroyl shikimate by 4CL and HCT, respectively. Then, C3′H catalyzes the production of caffeoyl shikimate, which can be used to produce caffeic acid by caffeoyl shikimate esterase (CSE) (Vanholme et al., 2013). The enzymes were detected in the ER. *A. thaliana* C3′H (CYP98A3) and C4H (CYP73A5) were shown to colocalize and dimerize in the ER of the transfected *N. benthamiana* leaf, and to associate with HCT and 4CL1 as soluble partners to form an enzyme complex of the phenylpropanoid pathway (Bassard et al., 2012). This suggests that their ER localization is pivotal to efficiently channel metabolites between the branches. Future studies are required to show whether these enzymes are part of a metabolon in Amaryllidaceae plants.

At expression levels, transcripts also shared similar tissue repartition. *PAL*, *C4H*, *C3′H*, and *TYDC1* from *L. aestivum* showed highest relative expression levels in roots, in which the precursors L-tyrosine, tyramine, and L-phenylalanine were detected. Their co-expression pattern is consistent with the hypothesis that they could complex together to form a metabolon. In *L. radiata*, gene expression analysis revealed higher *PAL* and *C4H* expression in root tissues compared to bulb and leaf (Li et al., 2018c). Interestingly, the products of phenylpropanoid enzymes, such as *p*-coumaric acid, caffeic acid, and ferulic acid, were predominantly detected in flowers. AA biosynthetic genes (*NBS*, *NR* and *N4′OMT*) were expressed in all tissues, but particularly abundant in bulbs and flowers. In this latter tissue, in addition to the phenylpropanoid precursors necessary for AA synthesis, 4′-*O*-methylnorbelladine, lycorine, haemanthamine, narciclasine, norgalanthamine, vittatine, and 11-hydroxy-vittatine were all detected. Our finding supports an inverse correlation of the upstream phenylpropanoid genes expression pattern with the phenylpropanoid and alkaloid metabolites content in the same tissue (Li et al., 2018a). Inter- and intra-cellular transport of phenylpropanoid compounds between cell compartments and also different cell types could occur between different tissues of the Amaryllidaceae plant (Biała and Jasiński, 2018). To our knowledge, nothing has been reported on the transport or single-cell multi-omics in Amaryllidaceae which could help elucidate further alkaloid metabolism in this plant family.

The phenylpropanoid pathway also catalyzes the formation of the precursors of lignin, lignans, flavonoids, and alkaloids in Amaryllidaceae. Screening for and identifying the *Lae*C4H and *Lae*C3′H genes are of great importance for elucidating AA metabolism in *L. aestivum*.

## 5. Conclusion

In the present study, we identified C4H, APX/C3H and C3′H in the *L. aestivum* transcriptome. The sequences of *Lae*C4H and *Lae*C3′H shared high identity with *bona fide* C4Hs and C3′H enzymes from several species and harbored typical CYP450 domains. The recombinant *Lae*C4H and *Lae*C3′H proteins were successfully expressed in yeast. *Lae*C4H catalyzed the expected 4-hydroxylation of *trans*-cinnamic to *p*-coumaric acid, whereas *Lae*C3′H catalyzed the 3-hydroxylation of *p*-coumaroyl shikimate to caffeoyl shikimate. *Lae*APX/C3H used *p*-coumaric acid as substrate but did not form caffeic acid. This work unravels the reactions involved in the first key steps of the biosynthesis of AAs. Deciphering AA precursor biosynthesis will facilitate the development of the biosynthetic tools required to produce AAs *in vitro* and help produce important pharmaceuticals, such as galanthamine, heterologous hosts to treat the symptoms of Alzheimer's disease.

## CRediT authorship contribution statement

**Vahid Karimzadegan:** Writing – review & editing, Writing – original draft, Visualization, Validation, Methodology, Investigation, Formal analysis, Conceptualization. **Manoj Koirala:** Writing – review & editing, Validation, Resources, Methodology. **Sajjad Sobhanverdi:** Writing – review & editing, Visualization, Validation, Methodology, Investigation, Formal analysis. **Natacha Merindol:** Writing – review & editing, Writing – original draft, Visualization, Resources, Project administration, Methodology, Formal analysis, Conceptualization. **Bharat Bhusan Majhi:** Writing – review & editing, Resources, Methodology. **Sarah-Eve Gélinas:** Writing – review & editing, Resources, Methodology, Formal analysis. **Vitaliy I. Timokhin:** Writing – review & editing, Resources, Methodology. **John Ralph:** Writing – review & editing, Resources, Methodology. **Mehran Dastmalchi:** Methodology, Supervision, Writing – review & editing. **Isabel Desgagné-Penix:** Conceptualization, Funding acquisition, Project administration, Resources, Supervision, Writing – original draft, Writing – review & editing.

## Declaration of competing interest

The authors declare that they have no known competing financial interests or personal relationships that could have appeared to influence the work reported in this paper.

## Data availability

Data will be made available on request.

## Acknowledgments

The authors wish to thank Professor Yang Qu (University of New Brunswick, Fredericton, NB, Canada) for generously providing yeast vector pESC-LEU-*Cro*CPR for protein expression. We also wish to give warms thanks to Dr. Elisa Fantino for precious technical advice during this study, and Mélodie B. Plourde and Snehi Gazal for their kind technical assistance and patience with confocal microscopy acquisition and analyses. We extend our thanks to the reviewers and editors for their careful reading and helpful comments on this manuscript. This work was supported by the Natural Sciences and Engineering Research Council of Canada (NSERC) award number RGPIN-2021-03218 to I. D-P; and the Canada Research Chair on plant specialized metabolism Award No CRC-2018-03218 to I. D-P. Many thanks are extended to the Canadian taxpayers and to the Canadian government for supporting the Canada Research Chairs Program. V.I.T. and J.R. were supported by the Great Lakes Bioenergy Research Center (US Department of Energy, Office of Science Biological and Environmental Research Program under Award Number DE-SC0018409).

## Appendix A. Supplementary data

Supplementary data to this article can be found online at https://doi.org/10.1016/j.plaphy.2024.108612.

## References

Achnine, L., Blancaflor, E.B., Rasmussen, S., Dixon, R.A., 2004. Colocalization of L-phenylalanine ammonia-lyase and cinnamate 4-hydroxylase for metabolic channeling in phenylpropanoid biosynthesis. Plant Cell 16, 3098–3109.

Adasme, M.F., Linnemann, K.L., Bolz, S.N., Kaiser, F., Salentin, S., Haupt, V.J., Schroeder, M., 2021. Plip 2021: expanding the scope of the protein-ligand interaction profiler to DNA and RNA. Nucleic Acids Res. 49, W530–W534.

Alber, A.V., Renault, H., Basilio-Lopes, A., Bassard, J.E., Liu, Z., Ullmann, P., Lesot, A., Bihel, F., Schmitt, M., Werck-Reichhart, D., Ehlting, J., 2019. Evolution of coumaroyl conjugate 3-hydroxylases in land plants: lignin biosynthesis and defense. Plant J. 99, 924–936.

Baek, M., DiMaio, F., Anishchenko, I., Dauparas, J., Ovchinnikov, S., Lee, G.R., Wang, J., Cong, Q., Kinch, L.N., Schaeffer, R.D., Millan, C., Park, H., Adams, C., Glassman, C. R., DeGiovanni, A., Pereira, J.H., Rodrigues, A.V., van Dijk, A.A., Ebrecht, A.C., Opperman, D.J., Sagmeister, T., Buhlheller, C., Pavkov-Keller, T., Rathinaswamy, M. K., Dalwadi, U., Yip, C.K., Burke, J.E., Garcia, K.C., Grishin, N.V., Adams, P.D.,

Read, R.J., Baker, D., 2021. Accurate prediction of protein structures and interactions using a three-track neural network. Science 373, 871–876.
Barros, J., Escamilla-Trevino, L., Song, L., Rao, X., Serrani-Yarce, J.C., Palacios, M.D., Engle, N., Choudhury, F.K., Tschaplinski, T.J., Venables, B.J., 2019. 4-Coumarate 3-hydroxylase in the lignin biosynthesis pathway is a cytosolic ascorbate peroxidase. Nat. Commun. 10, 1994.
Bassard, J.E., Richert, L., Geerinck, J., Renault, H., Duval, F., Ullmann, P., Schmitt, M., Meyer, E., Mutterer, J., Boerjan, W., De Jaeger, G., Mely, Y., Goossens, A., Werck-Reichhart, D., 2012. Protein-protein and protein-membrane associations in the lignin pathway. Plant Cell 24, 4465–4482.
Berkov, S., Georgieva, L., Kondakova, V., Atanassov, A., Viladomat, F., Bastida, J., Codina, C., 2009. Plant sources of galanthamine: phytochemical and biotechnological aspects. Biotechnol. Biotechnol. Equip. 23, 1170–1176.
Biała, W., Jasiński, M., 2018. The phenylpropanoid case–it is transport that matters. Front. Plant Sci. 9, 1610.
Chen, H.C., Li, Q., Shuford, C.M., Liu, J., Muddiman, D.C., Sederoff, R.R., Chiang, V.L., 2011. Membrane protein complexes catalyze both 4- and 3-hydroxylation of cinnamic acid derivatives in monolignol biosynthesis. Proc. Natl. Acad. Sci. U. S. A. 108, 21253–21258.
Desgagné-Penix, I., 2021. Biosynthesis of alkaloids in Amaryllidaceae plants: a review. Phytochemistry Rev. 20, 409–431.
Diamond, A., Desgagne-Penix, I., 2016. Metabolic engineering for the production of plant isoquinoline alkaloids. Plant Biotechnol. J. 14, 1319–1328.
Duvaud, S., Gabella, C., Lisacek, F., Stockinger, H., Ioannidis, V., Durinx, C., 2021. Expasy, the Swiss bioinformatics resource portal, as designed by its users. Nucleic Acids Res. 49, W216–W227.
Frederick, R.D., Thilmony, R.L., Sessa, G., Martin, G.B., 1998. Recognition specificity for the bacterial avirulence protein AvrPto is determined by Thr-204 in the activation loop of the tomato Pto kinase. Mol. Cell 2, 241–245.
Girard, M.P., Merindol, N., Berthoux, L., Desgagne-Penix, I., 2022. [Antiviral properties of plant alkaloids against RNA viruses]. Virologie 26, 431–450.
Hansen, C.C., Nelson, D.R., Møller, B.L., Werck-Reichhart, D., 2021. Plant cytochrome P450 plasticity and evolution. Mol. Plant 14, 1244–1265.
Havelek, R., Seifrtova, M., Kralovec, K., Bruckova, L., Cahlikova, L., Dalecka, M., Vavrova, J., Rezacova, M., Opletal, L., Bilkova, Z., 2014. The effect of Amaryllidaceae alkaloids haemanthamine and haemanthidine on cell cycle progression and apoptosis in p53-negative human leukemic Jurkat cells. Phytomedicine 21, 479–490.
Holsters, M., Silva, B., Van Vliet, F., Genetello, C., De Block, M., Dhaese, P., Depicker, A., Inze, D., Engler, G., Villarroel, R., et al., 1980. The functional organization of the nopaline *A. tumefaciens* plasmid pTiC58. Plasmid 3, 212–230.
Hotchandani, T., Desgagne-Penix, I., 2017. Heterocyclic Amaryllidaceae alkaloids: biosynthesis and pharmacological applications. Curr. Top. Med. Chem. 17, 418–427.
Hotze, M., Schröder, G., Schröder, J., 1995. Cinnamate 4-hydroxylase from *Catharanthus roseus* and a strategy for the functional expression of plant cytochrome P450 proteins as translational fusions with P450 reductase in *Escherichia coli*. FEBS Lett. 374, 345–350.
Hu, Y., Gai, Y., Yin, L., Wang, X., Feng, C., Feng, L., Li, D., Jiang, X.-N., Wang, D.-C., 2010. Crystal structures of a Populus tomentosa 4-coumarate: CoA ligase shed light on its enzymatic mechanisms. Plant Cell 22, 3093–3104.
Jayawardena, T.U., Merindol, N., Liyanage, N.S., Desgagné-Penix, I., 2024. Unveiling Amaryllidaceae alkaloids: from biosynthesis to antiviral potential – a review. Nat. Prod. Rep. https://doi.org/10.1039/D3NP00044C.
Ka, S., Merindol, N., Koirala, M., Desgagne-Penix, I., 2020. Biosynthesis and biological activities of newly discovered Amaryllidaceae alkaloids. Molecules 25, 4901.
Kelley, L.A., Mezulis, S., Yates, C.M., Wass, M.N., Sternberg, M.J., 2015. The Phyre2 web portal for protein modeling, prediction and analysis. Nat. Protoc. 10, 845–858.
Khatri, P., Chen, L., Rajcan, I., Dhaubhadel, S., 2023. Functional characterization of Cinnamate 4-hydroxylase gene family in soybean (*Glycine max*). PLoS One 18, e0285698.
Koirala, M., Karimzadegan, V., Liyanage, N.S., Mérindol, N., Desgagné-Penix, I., 2022. Biotechnological approaches to optimize the production of Amaryllidaceae alkaloids. Biomolecules 12, 893.
Kriegshauser, L., Knosp, S., Grienenberger, E., Tatsumi, K., Gütle, D.D., Sørensen, I., Herrgott, L., Zumsteg, J., Rose, J.K., Reski, R., 2021. Function of the HYDROXYCINNAMOYL-CoA: SHIKIMATE HYDROXYCINNAMOYL TRANSFERASE is evolutionarily conserved in embryophytes. Plant Cell 33, 1472–1491.
Li, W., Yang, L., Jiang, L., Zhang, G., Luo, Y., 2016. Molecular cloning and functional characterization of a cinnamate 4-hydroxylase-encoding gene from Camptotheca acuminata. Acta Physiol. Plant. 38, 1–9.
Li, W., Yang, Y., Qiao, C., Zhang, G., Luo, Y., 2018a. Functional characterization of phenylalanine ammonia-lyase-and cinnamate 4-hydroxylase-encoding genes from *Lycoris radiata*, a galanthamine-producing plant. Int. J. Biol. Macromol. 117, 1264–1279.
Li, Y., Li, J., Qian, B., Cheng, L., Xu, S., Wang, R., 2018b. De novo biosynthesis of p-coumaric acid in E. coli with a trans-cinnamic acid 4-hydroxylase from the Amaryllidaceae plant Lycoris aurea. Molecules 23.
Li, W., Yang, Y., Qiao, C., Zhang, G., Luo, Y., 2018c. Functional characterization of phenylalanine ammonia-lyase- and cinnamate 4-hydroxylase-encoding genes from Lycoris radiata, a galanthamine-producing plant. Int. J. Biol. Macromol. 117, 1264–1279.
Li, G., Liu, X., Zhang, Y., Muhammad, A., Han, W., Li, D., Cheng, X., Cai, Y., 2020. Cloning and functional characterization of two cinnamate 4-hydroxylase genes from Pyrus bretschneideri. Plant Physiol. Biochem. 156, 135–145.
Liu, J., Hu, W.X., He, L.F., Ye, M., Li, Y., 2004. Effects of lycorine on HL-60 cells via arresting cell cycle and inducing apoptosis. FEBS Lett. 578, 245–250.
Liu, Z., Tavares, R., Forsythe, E.S., André, F., Lugan, R., Jonasson, G., Boutet-Mercey, S., Tohge, T., Beilstein, M.A., Werck-Reichhart, D., 2016. Evolutionary interplay between sister cytochrome P450 genes shapes plasticity in plant metabolism. Nat. Commun. 7, 13026.
Liu, X.Y., Yu, H.N., Gao, S., Wu, Y.F., Cheng, A.X., Lou, H.X., 2017. The isolation and functional characterization of three liverwort genes encoding cinnamate 4-hydroxylase. Plant Physiol. Biochem. 117, 42–50.
Majhi, B.B., Gelinas, S.E., Merindol, N., Ricard, S., Desgagne-Penix, I., 2023. Characterization of norbelladine synthase and noroxomaritidine/norcraugsodine reductase reveals a novel catalytic route for the biosynthesis of Amaryllidaceae alkaloids including the Alzheimer's drug galanthamine. Front. Plant Sci. 14, 1231809.
Matsuno, M., Compagnon, V., Schoch, G.A., Schmitt, M., Debayle, D., Bassard, J.E., Pollet, B., Hehn, A., Heintz, D., Ullmann, P., Lapierre, C., Bernier, F., Ehlting, J., Werck-Reichhart, D., 2009. Evolution of a novel phenolic pathway for pollen development. Science 325, 1688–1692.
Morant, M., Schoch, G.A., Ullmann, P., Ertunc, T., Little, D., Olsen, C.E., Petersen, M., Negrel, J., Werck-Reichhart, D., 2007. Catalytic activity, duplication and evolution of the CYP98 cytochrome P450 family in wheat. Plant Mol. Biol. 63, 1–19.
Nelson, D.R., Strobel, H.W., 1988. On the membrane topology of vertebrate cytochrome P-450 proteins. J. Biol. Chem. 263, 6038–6050.
Padmakshan, D., Timokhin, V.I., Lu, F., Schatz, P.F., Vanholme, R., Boerjan, W., Ralph, J., 2022. Synthesis of hydroxycinnamoyl shikimates and their role in monolignol biosynthesis. Holzforschung 76, 133–144.
Pfaffl, M.W., 2001. A new mathematical model for relative quantification in real-time RT-PCR. Nucleic Acids Res. 29, e45.
Plewczynski, D., Łazniewski, M., Augustyniak, R., Ginalski, K., 2011. Can we trust docking results? Evaluation of seven commonly used programs on PDBbind database. J. Comput. Chem. 32, 742–755.
Pompon, D., Louerat, B., Bronine, A., Urban, P., 1996. Yeast expression of animal and plant P450s in optimized redox environments. In: Johnson, E.F., Waterman, M.R. (Eds.), Methods in Enzymology. Academic Press, pp. 51–64.
Ro, D.K., Mah, N., Ellis, B.E., Douglas, C.J., 2001. Functional characterization and subcellular localization of poplar (*Populus trichocarpa* x *Populus deltoides*) cinnamate 4-hydroxylase. Plant Physiol. 126, 317–329.
Schilmiller, A.L., Stout, J., Weng, J.K., Humphreys, J., Ruegger, M.O., Chapple, C., 2009. Mutations in the cinnamate 4-hydroxylase gene impact metabolism, growth and development in Arabidopsis. Plant J. 60, 771–782.
Schoch, G., Goepfert, S., Morant, M., Hehn, A., Meyer, D., Ullmann, P., Werck-Reichhart, D., 2001. CYP98A3 from Arabidopsis thaliana is a 3′-hydroxylase of phenolic esters, a missing link in the phenylpropanoid pathway. J. Biol. Chem. 276, 36566–36574.
Sen, K., Thiel, W., 2014. Role of two alternate water networks in Compound I formation in P450eryF. J. Phys. Chem. B 118, 2810–2820.
Sterling, T., Irwin, J.J., 2015. ZINC 15–ligand discovery for everyone. J. Chem. Inf. Model. 55, 2324–2337.
Szczesnaskorupa, E., Straub, P., Kemper, B., 1993. Deletion of a conserved tetrapeptide, PPGP, in P450 2C2 results in loss of enzymatic activity without a change in its cellular location. Arch. Biochem. Biophys. 304, 170–175.
Tallini, L.R., Osorio, E.H., Santos, V.D.D., Borges, W.S., Kaiser, M., Viladomat, F., Zuanazzi, J.A.S., Bastida, J., 2017. *Hippeastrum reticulatum* (Amaryllidaceae): alkaloid profiling, biological activities and molecular docking. Molecules 22, 4901.
Tamura, K., Stecher, G., Kumar, S., 2021. MEGA11: molecular evolutionary genetics analysis version 11. Mol. Biol. Evol. 38, 3022–3027.
Teutsch, H.G., Hasenfratz, M.P., Lesot, A., Stoltz, C., Garnier, J.M., Jeltsch, J.M., Durst, F., Werck-Reichhart, D., 1993. Isolation and sequence of a cDNA encoding the Jerusalem artichoke cinnamate 4-hydroxylase, a major plant cytochrome P450 involved in the general phenylpropanoid pathway. Proc. Natl. Acad. Sci. U. S. A. 90, 4102–4106.
Tousignant, L., Diaz-Garza, A.M., Majhi, B.B., Gelinas, S.E., Singh, A., Desgagne-Penix, I., 2022. Transcriptome analysis of *Leucojum aestivum* and identification of genes involved in norbelladine biosynthesis. Planta 255, 30.
Uhlmann, A., Ebel, J., 1993. Molecular cloning and expression of 4-coumarate: coenzyme A ligase, an enzyme involved in the resistance response of soybean (Glycine max L.) against pathogen attack. Plant Physiol. 102, 1147–1156.
Vanholme, R., Cesarino, I., Rataj, K., Xiao, Y., Sundin, L., Goeminne, G., Kim, H., Cross, J., Morreel, K., Araujo, P., 2013. Caffeoyl shikimate esterase (CSE) is an enzyme in the lignin biosynthetic pathway in *Arabidopsis*. Science 341, 1103–1106.
Werck-Reichhart, D., Feyereisen, R., 2000. Cytochromes P450: a success story. Genome Biol. 1, REVIEWS3003.
Xue, Y., Zhang, Y., Grace, S., He, Q., 2014. Functional expression of an Arabidopsis p450 enzyme, p-coumarate-3-hydroxylase, in the cyanobacterium Synechocystis PCC 6803 for the biosynthesis of caffeic acid. J. Appl. Phycol. 26, 219–226.
Zhang, B., Lewis, K.M., Abril, A., Davydov, D.R., Vermerris, W., Sattler, S.E., Kang, C., 2020. Structure and function of the cytochrome P450 monooxygenase cinnamate 4-hydroxylase from sorghum bicolor. Plant Physiol. 183, 957–973.
Zhang, J., Hansen, L.G., Gudich, O., Viehrig, K., Lassen, L.M.M., Schrubbers, L., Adhikari, K.B., Rubaszka, P., Carrasquer-Alvarez, E., Chen, L., D'Ambrosio, V., Lehka, B., Haidar, A.K., Nallapareddy, S., Giannakou, K., Laloux, M., Arsovska, D., Jorgensen, M.A.K., Chan, L.J.G., Kristensen, M., Christensen, H.B., Sudarsan, S., Stander, E.A., Baidoo, E., Petzold, C.J., Wulff, T., O'Connor, S.E., Courdavault, V.,

Jensen, M.K., Keasling, J.D., 2022. A microbial supply chain for production of the anti-cancer drug vinblastine. Nature 609, 341–347.
Zhang, B., Lewis, J.A., Vermerris, W., Sattler, S.E., Kang, C., 2023a. A sorghum ascorbate peroxidase with four binding sites has activity against ascorbate and phenylpropanoids. Plant Physiol. 192, 102–118.

Zhang, B., Lewis, J.A., Vermerris, W., Sattler, S.E., Kang, C., 2023b. A sorghum ascorbate peroxidase with four binding sites has activity against ascorbate and phenylpropanoids. Plant Physiol. 192, 102–118.